The Brazilian Society of Mechanical Sciences and Engineering

ABCM SYMPOSIUM SERIES IN MECHATRONICS

Vol. 1

Editors
Julio Cezar Adamowski
Edilson Hiroshi Tamai
Emília Villani
Paulo Eigi Miyagi

Published by ABCM – Brazilian Society of Mechanical Sciences and Engineering
Rio de Janeiro, RJ, Brazil
2004

ISBN 85-857699-20-3

ABCM Symposium Series in Mechatronics - Vol. 1 - pp.76-85
Copyright © 2004 by ABCM

IMPROVING THE POSITIONING ACCURACY OF ROBOTIC MANIPULATORS SUBJECT TO BASE OSCILLATIONS

Vivek Anand Sujan
Department of Mechanical Engineering, Massachusetts Institute of Technology
77 Massachusetts Avenue, Cambridge, MA 02139-4307, USA
e-mail: vasujan@mit.edu

Marco Antonio Meggiolaro
Department of Mechanical Engineering, Pontifical Catholic University of Rio de Janeiro
R. Marquês de São Vicente 225, Rio de Janeiro, RJ 22453-900, Brazil
e-mail: meggi@mec.puc-rio.br

Abstract. *Several robotic system applications require manipulators to carry heavy payloads while operating from moving vehicles. These manipulators are mounted on moving/compliant bases, introducing additional degrees of freedom that are not actuated, increasing the complexity of the dynamic modeling and control. In this paper, a control strategy to improve the performance of mobile robotic manipulators is presented. In the proposed architecture, a joint level controller needs to be designed to account for gravity, base motions, and manipulator joint friction. This is achieved by combining two methods: (i) a linear feed-forward dynamic disturbance compensation (DDC) method, which combines a dynamic model of the physical system with sensory feedback of the base oscillations to compensate for inertial effects; and (ii) Base Sensor Control, which compensates for nonlinear joint characteristics such as high joint friction. To evaluate the performance of the control architecture, a 3 DOF planar mobile manipulator is simulated including base oscillations, several payload weights, and Coulomb and viscous joint friction effects.*

Keywords: *robotics, control, dynamic compensation, joint friction.*

1. Introduction

Future mobile field robotic systems, such as planetary and terrestrial mission robots, will be required to perform complex tasks (Shaffer and Stentz, 1992). Planetary robots will be used to collect rock samples, to build infrastructures, and explore complex terrains. Tasks for terrestrial field robots may include explosive ordinance removal, de-mining and handling hazardous waste, and environment restoration (Baumgartner et al., 1998; Osborn, 1989; Shaffer and Stentz, 1992). This will require the handling of relatively large objects, such as deploying of solar panels and sensor arrays, anchoring of deployed structures, movement of rocks, and clearing of terrain. An important goal of robotics research is to develop mobile robots that can work in unstructured field environments, such as shown conceptually in Fig. (1) (Baumgartner et al., 1998). These robots consist basically of a manipulator attached to a deployment system (vehicle), which typically exhibits compliance due to its mechanical nature. Once the vehicle has approached a target position and has parked itself, the manipulator can then perform its tasks. The field robot may be equipped with a manipulator arm and sensors such as inclinometers, accelerometers, vision systems, and force/torque sensors, used to construct environment and task models from available sensory information. A number of problems can make this difficult. These include the uncertainty of the task in the environment, location and orientation errors in the robots, sensing occlusions, and external disturbances. Previously reported work has addressed problems due to environment and task sensing uncertainty and limitations (Sujan, 2002a; Sujan, 2002b; Sujan and Dubowsky, 2002).

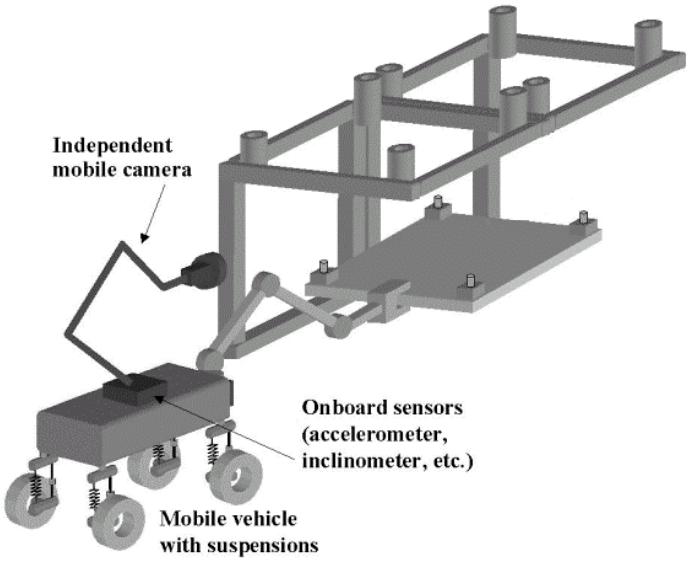

Figure 1. Representative physical system.

However, disturbances can significantly degrade the performance of such manipulators, arising due to robot-environment interaction forces and base compliance. They may cause the manipulator to leave its prescribed path, saturate its actuators, and induce high stresses (both internal and external e.g. at the endpoint). Additionally, a critical element in task execution may be the stresses exerted by the system on the structural elements and the environment. Therefore, these forces will have to be monitored and kept below a damage threshold during the entire task. The control of such systems typically requires models of the environment and task.

Several control architectures have been considered to perform manipulation tasks on compliant bases. PID (Proportional-Integral-Derivative) accurately maintains a set-point by adjusting the control outputs (Asada et al., 1986; Ogata, 2002). Proportional control outputs a feedback signal linearly proportional to the error in the measured output, reducing the rise time, but allowing for a non-zero steady state error. When the controller includes a term proportional to the integral of the error, then the steady state error can be eliminated, although this comes at the expense of deterioration in the dynamic system response. Finally, addition of a term proportional to the derivative of the error will have the effect of increasing the stability of the system, reducing the overshoot, and improving the transient response. However, classical PID control may have a very poor performance in the presence of significant non-linearities in the system.

Another typical control architecture is *robust control*, in which the problem of tracking a desired input and rejecting an unknown disturbance can be seen as an exercise in designing a control law to provide regulation of the error (Ogata, 2002). The control must also be structurally stable or robust, in the sense that regulation of error to zero in the steady state occurs even in the presence of small perturbations of the original system parameters. Note that in practice there is never a perfect model of the plant and the values of the parameters are always subject to some change. Several control structures have been developed to accomplish robust control, including H_2, H_∞, Linear Quadratic Regulator (LQR) and others.

Fuzzy logic in control has also been successfully used, in special to capture heuristic control laws obtained from human experience or engineering practice in automated algorithms (Klir et al., 1995). These control laws are defined by means of linguistic rules, e.g. “if the pressure is high, then decrease the pump power”. The heuristic approach in the controller design can be appealing for its simplicity, but formal design method can be mandatory in some cases.

In many process control applications, however, the dynamics may be too complex or the physical process is not well understood. The quantitative knowledge of the process is then not available. In these cases, a *neural network* can be selected because it generates a neural model without any detailed information regarding the internal working of the plant (Haykin, 1998). It can be used even for systems that are too complex for an accurate system model to be derived. A feed-forward architecture with a back-propagation learning algorithm is used due to its performance, accuracy, and relatively easy implementation. The neural net plant emulator is first trained to emulate a theoretical model of the nonlinear plant. A discrete theoretical model of the plant dynamics in state-space notation is used to choose the current states of the plant and the plant input (control command) as the input to the emulator. The next states, after one sample period, are chosen as the output. During the learning procedure, the errors between the actual network output and the desired values are minimized, by upgrading the weights. After training, the neural emulator perfectly predicts the next states (delayed by one sample time) of the plant for the current states and control command. However, such control strategy is usually very expensive computationally.

Adaptive algorithms (Slotine et al., 1991) have been developed for tuning control parameters in the presence of system uncertainties and/or on line parameter variations, such as in the case of base oscillations. In explicit or indirect adaptive control, an identifier must be implemented to give estimates of these unknown parameters; these parameters are then used for control computation. In implicit or direct adaptive control, the control gains are computed without need for the intermediate identification procedure. One particular procedure that is especially attractive for multiple input multiple output systems is *model reference adaptive control* (MRAC). However, in order to guarantee perfect tracking, certain positivity conditions need to be satisfied. Because direct MRAC procedures are easily implementable, various procedures have been developed for alleviating the satisfaction of these positivity conditions. However, model based self-tuning PID or identification-based adaptive controllers cannot provide adequate high-speed adaptive control because model training can be too time-consuming.

On the other hand, a very useful and inexpensive control method is model predictive control, where disturbance rejection is accomplished by estimating the equivalent disturbance of a system based on its dynamic model and the sensed disturbances. This is also known as feed-forward control, or Dynamic Disturbance Compensation (DDC). Disturbance measurements are fed into a dynamic system model, which are fed forward and added to the basic controller commands (Dubowsky et al., 1987; Hootsmans et al. 1992).

However, for high accuracy manipulator systems with large forces (e.g. due to endpoint payloads), achieving an adequate controller scheme may be difficult due to joint friction. Joint friction can lead to undesirable stick-slip behavior, leading to poor accuracy and large sudden manipulator motions. Friction compensation techniques in the literature typically require detailed friction models of the actuators and joints. They may also require the installation of costly and complex joint torque sensors in the system, which account for joint friction by measuring the actual joint torques. The difference between these readings and the expected input torques gives a direct reading for the joint friction torque.

To compensate for nonlinear joint characteristics in robotic manipulators, such as high joint friction, a simple and effective control method has been developed that is modeless and does not require internal joint sensors, known as Base Sensor Control (BSC). BSC estimates manipulator joint torques from a self-contained external six-axis force/torque

sensor placed under the manipulator's base. The joint torque estimates allow for accurate joint torque control that has been shown to greatly improve repeatability of both hydraulic and electric manipulators (Meggiolaro et al., 1999; Morel et al. 2000).

In this paper, the problem of disturbance compensation is addressed for mobile manipulators with compliant bases, by effectively combining both DDC and BSC methods. The basics of BSC are reviewed in the next section.

2. Base Sensor Control

The following is a brief review of the basis for BSC. The complete development is presented in (Meggiolaro et al., 1999; Morel et al. 2000). BSC has been developed to compensate for nonlinear joint characteristics in robotic manipulators, such as high joint friction, to improve system repeatability.

As shown in Fig. (2), the wrench, $\mathbf{W_b}$, exerted by the manipulator on its base sensor can be expressed as the sum of three components

$$\mathbf{W_b} = \mathbf{W_g} + \mathbf{W_d} + \mathbf{W_e} \tag{1}$$

where $\mathbf{W_g}$ is the robot gravity component, $\mathbf{W_d}$ is caused by manipulator motion, and $\mathbf{W_e}$ is the wrench exerted by the payload on the end-effector. Note that joint friction does not appear in the measured base sensor wrench, since it is an internal force. In the fine-motion case, it is assumed that the gravity wrench is essentially constant, and this wrench can be approximated by the initial value measured by the base sensor. The complexity of computing the gravitational wrench, such as identification of link weights and a static manipulator model, is eliminated. Under this assumption, the Newton Euler equations of the first i links are

$$\begin{cases} \mathbf{W_{0\to 1}} = -\mathbf{W_b} \\ \mathbf{W_{1\to 2}} = \mathbf{W_{0\to 1}} - \mathbf{W_{d_1}} \\ \vdots \\ \mathbf{W_{i\to i+1}} = \mathbf{W_{i-1\to i}} - \mathbf{W_{d_i}} \\ \vdots \\ -\mathbf{W_e} = \mathbf{W_{n-1\to n}} - \mathbf{W_{d_n}} \end{cases} \tag{2}$$

where $\mathbf{W_{i\to i+1}}$ is the wrench exerted by link *i* on link *i*+1, and $\mathbf{W_{d_i}}$ is the dynamic wrench for link *i*.

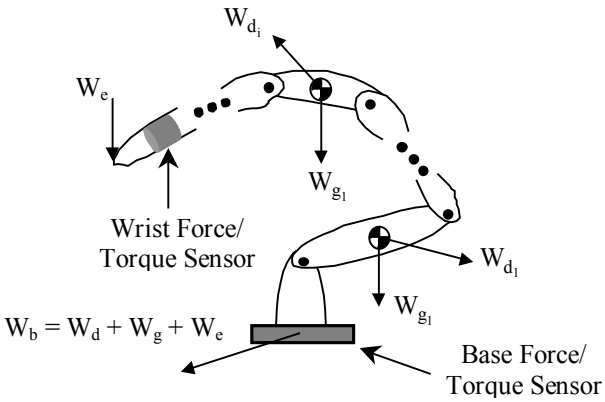

Figure 2. External and dynamic wrenches acting on each manipulator link.

For fine tasks it is assumed that the manipulator moves very slowly so that W_d can be neglected. Therefore, for slow, fine motions, only the measured wrench at the base is used to estimate the torque in joint *i*+1. The estimated torque in joint *i*+1 is obtained by projecting the moment vector at the origin O_i of the i^{th} reference frame along the joint axis z_i

$$\tau_{i+1} = -z_i^{\,T} \cdot \mathbf{W_b}^{O_i} \tag{3}$$

The value of τ_{i+1} depends only on the robot's kinematic parameters, joint angles and base sensor measurements.

With estimates of the joint torque, it is possible to achieve high performance torque control that can greatly reduce the effects of joint friction and non-linearities. This results in greatly improved repeatability. Figure (3) shows an application of BSC to a typical manipulator.

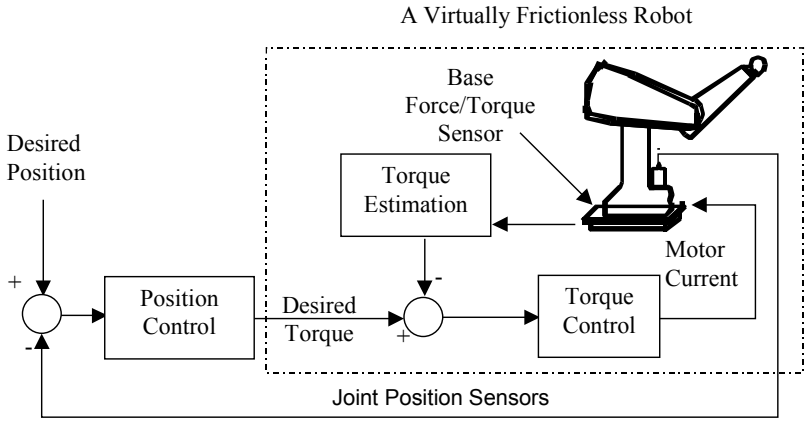

Figure 3. Base Sensor Control loop.

However, the BSC method will not compensate for sources of random repeatability errors, such as limited encoder resolution. In addition, a manipulator with good repeatability may not have fine absolute position accuracy. After improving the system repeatability using BSC, a model-based error correction method can be applied to reduce the absolute accuracy errors. Also, BSC assumes that the force/torque sensors are mounted on a rigid base. In the presence of base compliance, BSC must be combined with other control methods to compensate for external disturbances, as follows.

3. Control system design concept

After investigating several controller options, a BSC controller with model-predictive feed-forward compensation for disturbance rejection of mobile base motions has been selected, see Fig. (4).

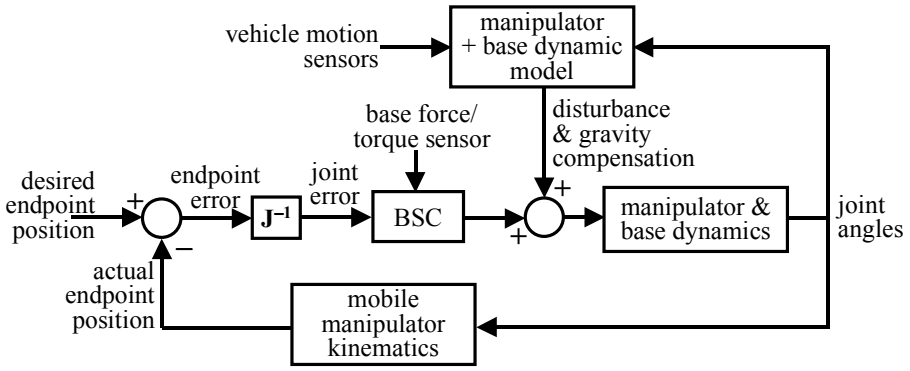

Figure 4. Block diagram of linear feed-forward compensation for dynamic disturbance rejection.

The sensor-based feed-forward compensation signals mitigate the external disturbances. Essentially the system measures the important disturbances, such as vehicle motions, and figures out what it needs to do to compensate for them. This controller decision is based on a dynamic model of the physical system, which requires the incorporation of several sensors used by the control algorithm. Such sensors provide the necessary data for the system to operate effectively. This data would include base motions (accelerations, inclinations), forces and torques applied within/to the system, obstacle presence, manipulator and wheel link angles, etc. The sensors required for this mission include (but are not limited to) joint and wheel encoders, wrist force/torque sensors, base force/torque sensors, vehicle motion sensors (accelerometers, gyros, inclinometers etc), acoustic sensors, vision sensors and strain gauges, which are used to estimate and then compensate for the expected deviations in joint angles/positions by simple feed-forward signals.

However, such a control scheme is dependent on obtaining a sufficiently accurate model of the manipulator and obtaining low noise sensory data. Degradation in the accuracy of the models and the disturbance measurements result in corresponding degradation of the controller.

Using a Lagrangian formulation, the dynamic model of the mobile manipulator system is developed. This model accounts for robot base motion and compliance (see Fig. (5) for a planar representation). The primary steps involved in this process are described as follows.

3.1. Reduction of suspension compliance system

A 6 DOF linear stiffness and damping system, located at the vehicle base center-of-gravity, represents its multi-element suspension system. For small base motions, this model of the suspension is sufficient to model the vehicle dynamics accurately. If the contributions to the suspension are known to occur only from the vehicle tires and a passive compliance element, then the combined 6 DOF stiffness at the center of gravity is given by

$$
\begin{aligned}
K^{x,y,z} &= \sum_i \left(\frac{1}{K^{x,y,z}_{suspension}} + \frac{1}{K^{x,y,z}_{wheel}} \right)^{-1}_i \\
K^{\theta_x} &= \sum_i \frac{K^z_i dz_i l_i \cdot \hat{z} + K^y_i dy_i dz_i}{tan^{-1}\left(\frac{dy_i}{dz_i}\right)} \\
K^{\theta_y} &= \sum_i \frac{K^z_i dz_i l_i \cdot \hat{z} + K^x_i dx_i dz_i}{tan^{-1}\left(\frac{dx_i}{dz_i}\right)} \\
K^{\theta_z} &= \sum_i \frac{K^y_i dy_i l_i \cdot \hat{y} + K^x_i dx_i dy_i}{tan^{-1}\left(\frac{dx_i}{dy_i}\right)}
\end{aligned}
\tag{4}
$$

where $K^{x,y,z}$ is the linear stiffness (in kN/m) in the x, y or z direction, K^{θ} is the angular stiffness (in kN·m/rad), and dx_i, dy_i and dz_i are the distances between the vehicle center of gravity and tire i in the x, y or z direction.

Similar expressions may be derived for the 6 DOF damping terms.

3.2 Robot model Lagrangian dynamics

In general, for a multi-DOF serial manipulator, the spatial equation of motion for the i[th] link is given by

$$Q_i - \left(\mathbf{J}^{\mathbf{T}}\mathbf{F}\right)_i = \sum_{j=1}^{n} H_{ij}\ddot{q}_j + \sum_{j=1}^{n}\sum_{k=1}^{n} h_{ijk}\dot{q}_j\dot{q}_k - G_i \tag{5}$$

$$\mathbf{H}_{nxn} = \sum_{i=1}^{n} m_i \mathbf{J}_L^{(i)T}\mathbf{J}_L^{(i)} + \mathbf{J}_A^{(i)T} I_i \mathbf{J}_A^{(i)} \tag{6}$$

$$h_{ijk} = \frac{\partial H_{ij}}{\partial q_k} - \frac{1}{2}\frac{\partial H_{jk}}{\partial q_i} \tag{7}$$

$$G_i = \sum_{j=1}^{n} m_j \mathbf{g}^T \mathbf{J}_{Li}^{(j)} \tag{8}$$

$$
\begin{aligned}
\mathbf{v}_{\mathbf{c_j}} = \mathbf{J}_L^{(j)} \cdot \dot{\mathbf{q}} \Rightarrow \mathbf{J}_{Li}^{(j)} &= \begin{cases} \mathbf{b_i} & \text{prismatic joint} \\ \mathbf{b_i} \times \mathbf{r_{i,c_j}} & \text{revolute joint} \end{cases} \\
\boldsymbol{\omega}_j = \mathbf{J}_A^{(j)} \cdot \dot{\mathbf{q}} \Rightarrow \mathbf{J}_{Ai}^{(j)} &= \begin{cases} \mathbf{0} & \text{prismatic joint} \\ \mathbf{b_i} & \text{revolute joint} \end{cases}
\end{aligned}
\tag{9}
$$

where

Q_i is the generalized force on joint i (in N or N·m);
q_i is the generalized coordinate associated to joint i (m or rad), element of the vector **q**;
H_{ij} is element (i, j) of the arm inertia matrix **H**;
h_{ijk} is Christoffel's three-index coefficient, an element of the augmented matrix **h**;
G is the gravitational term (N or N·m);
$\mathbf{J}^{(j)}$ is column j of the manipulator Jacobian matrix **J**, where A and L are relative to angular and linear velocities;
F is the manipulator endpoint external force (N);
m_i and I_i are the mass (kg) and moment of inertia (N·m^2) of link i;
g is the gravitational acceleration vector (m/s^2);

v_{cj} is the linear velocity (m/s) of the centroid of link j;
ω_j is the angular velocity (rad/s) of link j;
$\mathbf{b_i}$ is the 3x1 unit vector along joint axis i; and
$\mathbf{r_{i,c_j}}$ is the position vector (m) from the origin of the i^{th} frame to the centroid of link j.

For example, in the planar system shown in Fig. (5), the generalized variables **q** are given by

$$\mathbf{q} = [x_V \; y_V \; \theta_V \; x_S \; y_S \; \theta_S \; \theta_1 \; \theta_2 \; \theta_3]^T \tag{10}$$

where $[x_V, y_V, \theta_V]$ are the vehicle disturbance vector **d** (in the x, y and θ directions), $[x_S, y_S, \theta_S]$ are the vehicle chassis position and orientation, and θ_i are the manipulator joint angular displacements (in rad).

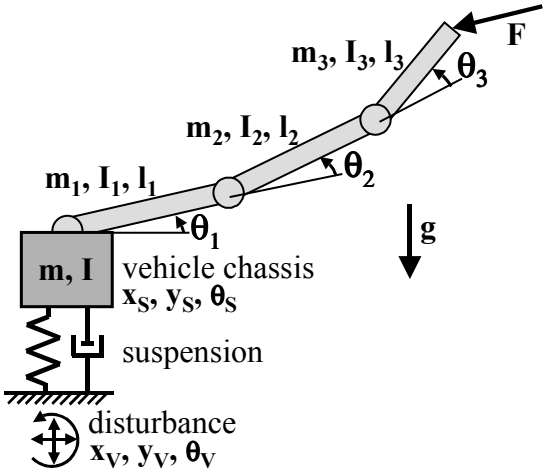

Figure 5. Mobile manipulator model including external endpoint forces.

Considering small perturbations Δq_i about an equilibrium state q_i^e and substituting into the non-linear dynamic equations of motion gives

$$\begin{aligned} & q_i = q_i^e + \Delta q_i \\ & \left(\dot{q}_i^e + \Delta\dot{q}_i\right)\left(\dot{q}_j^e + \Delta\dot{q}_j\right) = \dot{q}_i^e\dot{q}_j^e + \dot{q}_i^e\Delta\dot{q}_j + \dot{q}_j^e\Delta\dot{q}_i + \Delta\dot{q}_i\Delta\dot{q}_j \\ & \Rightarrow \mathbf{Q} - \mathbf{J}^T\mathbf{F} + \mathbf{G} - \hat{\mathbf{H}}(\mathbf{q}, \ddot{\mathbf{q}}^e) = \mathbf{H}\Delta\ddot{\mathbf{q}} + \hat{\mathbf{h}}(\mathbf{q}, \dot{\mathbf{q}}^e)\Delta\dot{\mathbf{q}} \end{aligned} \tag{11}$$

where the symbol ^ stands for estimated values.

Alternatively, these non-linear equations of motion may be simplified using Computed Torque Techniques, where

$$\begin{aligned} & Q_i - \left(\mathbf{J}^T\mathbf{F}\right)_i = \sum_{j=1}^{n} H_{ij}\ddot{q}_j + \sum_{j=1}^{n}\sum_{k=1}^{n} h_{ijk}\dot{q}_j\dot{q}_k - G_i \\ & Q_i^c \equiv Q_i - \left(\mathbf{J}^T\mathbf{F}\right)_i - \sum_{j=1}^{n}\sum_{k=1}^{n} h_{ijk}\dot{q}_j\dot{q}_k + G_i \\ & \Rightarrow \mathbf{Q^c} = \mathbf{H}\ddot{\mathbf{q}} \end{aligned} \tag{12}$$

As long as the left hand term $\mathbf{Q^c}$ can be computer in real time, the equations of motion have been linearized. Converting Eq. (12) into state-space form, then

$$\begin{aligned} & \dot{\mathbf{x}} = \mathbf{A}\mathbf{x} + \mathbf{B}\left(\mathbf{u} - \hat{\mathbf{F}}\left[\ddot{x}_V \;\; \ddot{y}_V \;\; \ddot{\theta}_V\right]^T\right) \\ & \mathbf{y} = \mathbf{C}\mathbf{x} + \mathbf{D}\mathbf{u} \end{aligned} \tag{13}$$

where $\hat{\mathbf{F}}$ is the inertial feed-forward term. Defining $\hat{\mathbf{f}}$ as the damping feed-forward term, then the simplified state-space equations for the planar system shown in Fig. (5), without considering the vehicle base motion, are

$$\mathbf{x} = \left[\theta_s \; x_s \; y_s \; \theta_1 \; \theta_2 \; \theta_3 \; \dot{\theta}_s \; \dot{x}_s \; \dot{y}_s \; \dot{\theta}_1 \; \dot{\theta}_2 \; \dot{\theta}_3\right]^T \tag{14}$$

$$\mathbf{u} = \left[Q^c_{\theta_s} \quad Q^c_{x_s} \quad Q^c_{y_s} \quad Q^c_1 \quad Q^c_2 \quad Q^c_3\right]^T = \left[\tau^c_{\theta_s} \quad F^c_{x_s} \quad F^c_{y_s} \quad \tau^c_1 \quad \tau^c_2 \quad \tau^c_3\right]^T \tag{15}$$

$$\mathbf{H} \equiv \begin{bmatrix} [\;]_{3x3} & [\;]_{3x6} \\ [\hat{\mathbf{F}}]_{6x3} & [\hat{\mathbf{H}}]_{6x6} \end{bmatrix} \qquad \mathbf{h} \equiv \begin{bmatrix} [\;]_{3x3} & [\;]_{3x6} \\ [\hat{\mathbf{f}}]_{6x3} & [\hat{\mathbf{h}}]_{6x6} \end{bmatrix} \tag{16}$$

$$\mathbf{A} = \begin{bmatrix} [0_{6x6}] & [I_{6x6}] \\ [0_{6x6}] & [0_{6x6}] \end{bmatrix} \; \mathbf{B} = \begin{bmatrix} [\;0_{6x6}\;] \\ [\;\hat{\mathbf{H}}^{-1}{}_{6x6}\;] \end{bmatrix} \; \mathbf{C} = [[I_{6x6}][0_{6x6}]] \; \mathbf{D} = [0]_{6x6} \tag{17}$$

3.3. Stability of the position controller

Using the above state-space formulation of the dynamic system model, the effects of disturbances may be predicted and compensated for. However, it is important to confirm that such a controller, seen in Fig. (4), will remain stable. For the planar 3 DOF arm system show in Fig. (5), the manipulator dynamics are now given by

$$\begin{bmatrix} \tau_1 \\ \tau_2 \\ \tau_3 \end{bmatrix} = \hat{\mathbf{H}} \begin{bmatrix} \ddot{\theta}_1 \\ \ddot{\theta}_2 \\ \ddot{\theta}_3 \end{bmatrix} + \hat{\mathbf{h}} \begin{bmatrix} \dot{\theta}_1 \\ \dot{\theta}_2 \\ \dot{\theta}_3 \end{bmatrix} + \hat{\mathbf{F}} \begin{bmatrix} \ddot{x}_V \\ \ddot{y}_V \\ \ddot{\theta}_V \end{bmatrix} + \hat{\mathbf{f}} \begin{bmatrix} \dot{x}_V \\ \dot{y}_V \\ \dot{\theta}_V \end{bmatrix} + \begin{bmatrix} G_1 \\ G_2 \\ G_3 \end{bmatrix} \tag{18}$$

$$\hat{\boldsymbol{\tau}} = \hat{\mathbf{H}}\ddot{\mathbf{q}} + \hat{\mathbf{h}}\dot{\mathbf{q}} + \hat{\mathbf{F}}\ddot{\mathbf{d}} + \hat{\mathbf{f}}\dot{\mathbf{d}} + \hat{\mathbf{G}}$$

where τ_i are the elements of the joint torque vector $\boldsymbol{\tau}$.

For a PD joint controller coupled with gravity compensation and dynamic disturbance rejection feed-forward terms, it is found that

$$\hat{\boldsymbol{\tau}} \equiv \mathbf{K}_P(\hat{\mathbf{q}}_\mathbf{r} - \hat{\mathbf{q}}) + \mathbf{K}_D(\dot{\hat{\mathbf{q}}}_\mathbf{r} - \dot{\hat{\mathbf{q}}}) + \hat{\mathbf{F}}\ddot{\mathbf{d}} + \hat{\mathbf{f}}\dot{\mathbf{d}} + \hat{\mathbf{G}} = -\mathbf{K}_P\tilde{\mathbf{q}} - \mathbf{K}_D\dot{\tilde{\mathbf{q}}} + \hat{\mathbf{F}}\ddot{\mathbf{d}} + \hat{\mathbf{f}}\dot{\mathbf{d}} + \hat{\mathbf{G}} \tag{19}$$

where $\mathbf{K_P}$ and $\mathbf{K_D}$ are the proportional and derivative control gain matrices, $\mathbf{q_r}$ is a (desired) reference state, and the symbol ~ stands for estimation errors.

The stability of this controller may be verified by considering the following Lyapunov function candidate

$$V(\mathbf{q}, \dot{\mathbf{q}}) = \frac{1}{2}\tilde{\mathbf{q}}^\mathbf{T}\mathbf{K_P}\tilde{\mathbf{q}} + \frac{1}{2}\dot{\mathbf{q}}^\mathbf{T}\mathbf{H}\dot{\mathbf{q}} \tag{20}$$

Since the matrices $\mathbf{K_P}$ and $\mathbf{H}$ are symmetric and positive definite, the Lyapunov function V is always positive (except when $\mathbf{q} = \mathbf{q_d}$). Differentiating V with respect to time gives

$$\begin{aligned} \dot{V} &= \tilde{\mathbf{q}}^\mathbf{T}\mathbf{K_p}\dot{\tilde{\mathbf{q}}} + \dot{\mathbf{q}}^\mathbf{T}\mathbf{H}\ddot{\mathbf{q}} + \frac{1}{2}\dot{\mathbf{q}}^\mathbf{T}\dot{\mathbf{H}}\dot{\mathbf{q}} = \tilde{\mathbf{q}}^\mathbf{T}\mathbf{K_P}\dot{\tilde{\mathbf{q}}} + \dot{\mathbf{q}}^\mathbf{T}(\boldsymbol{\tau} - \mathbf{h}\dot{\mathbf{q}} - \hat{\mathbf{F}}\ddot{\mathbf{d}} - \hat{\mathbf{f}}\dot{\mathbf{d}} - \mathbf{G}) + \frac{1}{2}\dot{\mathbf{q}}^\mathbf{T}\dot{\mathbf{H}}\dot{\mathbf{q}} \\ &= \tilde{\mathbf{q}}^\mathbf{T}\mathbf{K_P}\dot{\mathbf{q}} - \dot{\mathbf{q}}^\mathbf{T}(\mathbf{K_D}\dot{\tilde{\mathbf{q}}} + \mathbf{h}\dot{\mathbf{q}}) - \dot{\mathbf{q}}^\mathbf{T}\mathbf{K_P}\tilde{\mathbf{q}} + \frac{1}{2}\dot{\mathbf{q}}^\mathbf{T}\dot{\mathbf{H}}\dot{\mathbf{q}} \\ &= -\dot{\mathbf{q}}^\mathbf{T}(\mathbf{K_D} + \mathbf{h})\dot{\mathbf{q}} + \frac{1}{2}\dot{\mathbf{q}}^\mathbf{T}\dot{\mathbf{H}}\dot{\mathbf{q}} = -\dot{\mathbf{q}}^\mathbf{T}\mathbf{K_D}\dot{\mathbf{q}} + \frac{1}{2}\dot{\mathbf{q}}^\mathbf{T}(\dot{\mathbf{H}} - 2\mathbf{h})\dot{\mathbf{q}} = -\dot{\mathbf{q}}^\mathbf{T}\mathbf{K_D}\dot{\mathbf{q}} \le 0 \end{aligned} \tag{21}$$

If $\dot{V} = 0$ then $\dot{\mathbf{q}} = 0$, which leads to

$$\begin{aligned} &\ddot{\mathbf{q}} = \mathbf{H}^{-1}(\boldsymbol{\tau} - \mathbf{h}\dot{\mathbf{q}} - \hat{\mathbf{F}}\ddot{\mathbf{d}} - \hat{\mathbf{f}}\dot{\mathbf{d}} - \mathbf{G}) = \mathbf{H}^{-1}(-\mathbf{K_P}\tilde{\mathbf{q}} - \mathbf{K_D}\dot{\tilde{\mathbf{q}}} - \mathbf{h}\dot{\mathbf{q}}) = -\mathbf{H}^{-1}\mathbf{K_P}\tilde{\mathbf{q}} \\ &\therefore \ddot{\mathbf{q}} \neq 0, \text{if } \mathbf{q} \neq \mathbf{q}_\mathrm{d} \end{aligned} \tag{22}$$

Therefore, the Lyapunov stability criteria apply and the proposed controller is stable.

3.4. Dynamic tip-over stability

Once a dynamic model of the robotic system(s) has been set up, the controller needs to maintain tip-over stability (Takanishi et al., 1989). This is achieved by limiting the motion of the dynamic zero-moment point (*zmp*, or dynamic center of gravity) to lie within the vehicle footprint, see Fig. (6).

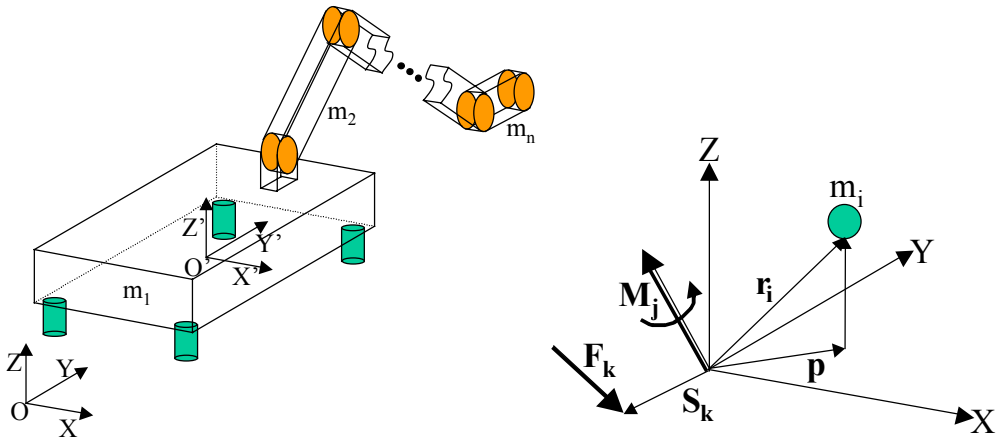

(a) General robot system (b) Force and moments on an individual mass element

Figure 6. Dynamic tip-over stability.

Using d'Alambert's principle, the forces/torques on each individual mass particle are evaluated. As seen in Fig. (6), the *X* and *Y* components of the zero moment point (*zmp*) are given by

$$\mathbf{T} = \sum_j \mathbf{M_j} - \sum_i m_i(\mathbf{r_i} - \mathbf{p}) \times (\ddot{\mathbf{r}}_\mathbf{i} + \mathbf{g}) + \sum_k (\mathbf{S_k} - \mathbf{p}) \times \mathbf{F_k}$$

$$X_{zmp} = \frac{\sum_{i=1}^{n} m_i(\ddot{z}_i + g_z)x_i - \sum_{i=1}^{n} m_i(\ddot{x}_i + g_x)z_i + \sum_j M_{y_j} + \sum_k \left(z_{S_k} F_{x_k} - x_{S_k} F_{z_k}\right)}{\sum_{i=1}^{n} m_i(\ddot{z}_i + g_z) - \sum_k F_{z_k}} \tag{23}$$

$$Y_{zmp} = \frac{\sum_{i=1}^{n} m_i(\ddot{z}_i + g_z)y_i - \sum_{i=1}^{n} m_i(\ddot{y}_i + g_y)z_i + \sum_j M_{x_j} + \sum_k \left(y_{S_k} F_{z_k} - z_{S_k} F_{y_k}\right)}{\sum_{i=1}^{n} m_i(\ddot{z}_i + g_z) - \sum_k F_{z_k}}$$

where

T is the total torque [T_x, T_y, T_z] acting on point p (N·m);
$\mathbf{M_j}$ is the externally applied moment [M_{xj}, M_{yj}, M_{zj}];
$\mathbf{F_k}$ is an externally applied force [F_{xk}, F_{yk}, F_{zk}];
$\mathbf{S_k}$ is the position vector [x_{S_k}, y_{S_k}, z_{S_k}] where external force $\mathbf{F_k}$ is applied;
$\mathbf{r_i}$ is the position vector [x_i, y_i, z_i] of particle i (with mass m_i);
p is the position vector [x_p, y_p, 0] of point p; and
g_x, g_y and g_z are components of the gravitational acceleration vector **g** (m/s^2).

The controller is able to determine the admissible robot motion states, by confining the position of the system zero moment point (X_{zmp}, Y_{zmp}) to within the vehicle footprint. Using the above dynamic models and a model predictive control architecture, the robot can execute the required tasks.

4. Simulation results

Simulations have been performed to verify the validity of the control methodologies developed in this paper. A planar model for the robotic system was used, consisting of a 3 DOF manipulator mounted on a compliant vehicle, see Fig. (5). The kinematics and dynamics of this rigid mobile manipulator influenced by the base motion were built into the simulation. The vehicle mass was assumed to be 10 kg, with moment of inertia 1.0 kg·m^2, and the base stiffness and

damping terms in all directions were 200 kN/m and 1.0 kN/(m/s), respectively. The manipulator parameters and control gains are shown in Table 1, where K_P, K_D and K_I are proportional, derivative and integral control gains.

Table 1 - Manipulator parameters and control gains used in the simulations.

	length	mass	inertia	PID control gains		
link	l_i (m)	m_i (kg)	I_i (kg·m^2)	K_P	K_D	K_I
1	0.813	5.0	0.523	80	7	0.25
2	0.508	3.0	0.360	110	6	1.0
3	0.508	3.0	0.360	150	9	1.0

Artificial base oscillations have been introduced as follows: roll of 11° and pitch of 2° with a 2s period (0.5 Hz). An end-point payload mass of 8 kg under a 9.81 m/s^2 gravity field was assumed. Figure (7) shows the data obtained for the manipulator position control. Although both cases include gravity compensation in the control loop, it is seen that when dynamic disturbance compensation was eliminated from the loop, the manipulator was unable to maintain a constant position due to the dynamic forces from the base oscillations. By introducing DDC into the control loop, the robot was then able to predict (from the manipulator dynamic model) the errors that would be introduced into the system due to the base motions. This feed-forward term, in addition to the PID control terms, allowed the manipulator to compensate for the dynamic disturbance.

Coulomb and viscous friction models of the manipulator joints have also been added to the simulation. Such models demonstrate system degradation due to friction. However, after replacing the PID control by BSC in the simulation, the friction effects were compensated for, resulting in endpoint position responses similar to the ones in Fig. (7).

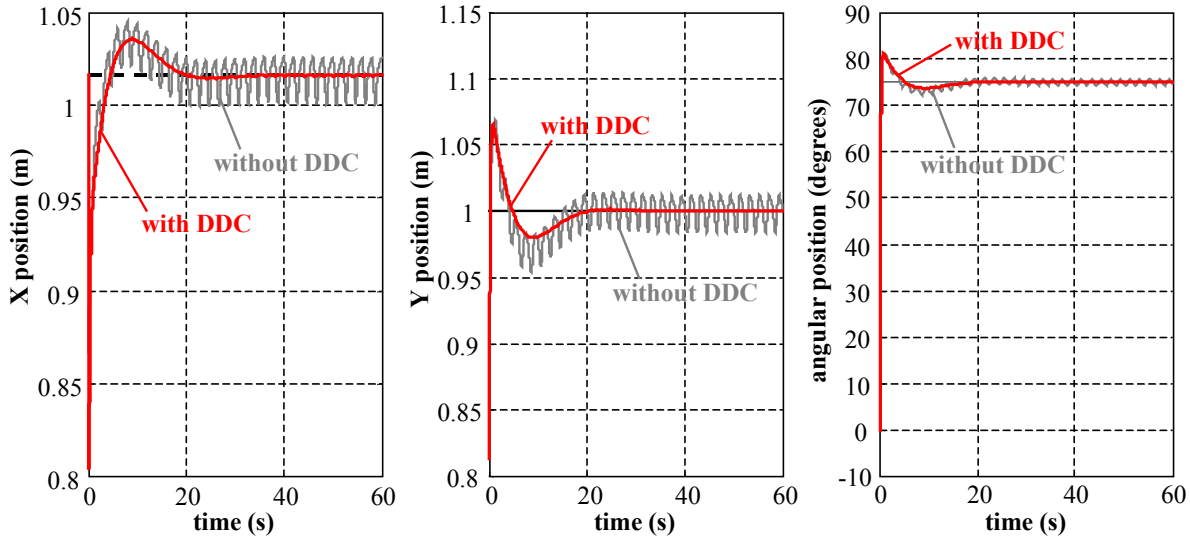

Figure 7. Simulation of endpoint position control of a manipulator with and without dynamic disturbance compensation (DDC).

5. Conclusions

This paper addressed the problem of disturbance compensation for the successful assembly of structures by mobile field robots. A control architecture, consisting of a linear PID joint controller with model predictive feed-forward compensation for mobile base motion disturbance rejection has been proposed. Issues presented include dynamic modeling of mobile manipulators, control architecture design, and stability analysis. The simulation results showed that conventional joint level PID control with gravity compensation was unable to maintain a constant payload position in the presence of base oscillations. By introducing DDC into the control loop, the robot was able to compensate for the dynamic disturbances due to base motions. In addition, the PID controller was replaced by Base Sensor Control to compensate for joint friction, allowing for accurate position control.

6. References

Asada, H., Slotine, J.J., 1986, "Robot Analysis and Control", J. Wiley & Sons.

Baumgartner, E.T., Schenker, P.S., Leger, C. and Huntsberger, T.L., 1998, "Sensor-Fused Navigation and Manipulation from a Planetary Rover", Proceedings of the SPIE Symposium on Sensor Fusion and Decentralized Control in Robotic Systems, Vol. 3523, Boston, MA, USA.

Dubowsky, S., Tanner, A.B., 1987, “A study of the dynamics and control of mobile manipulators subjected to vehicle disturbances”, Proceeding of the Fourth International Symposium of Robotics Research, Santa Cruz, CA.

Haykin, S.S., 1998, “Neural Networks: A Comprehensive Foundation”, Prentice Hall.

Hootsmans, N.A.M., Dubowsky, S., Mo, P.Z., 1992, “The experimental performance of a mobile manipulator control algorithm”, Proc. of the IEEE International Conference on Robotics and Automation, France, Vol.3, pp.1948-1954.

Klir, G.J., Yuan, B., 1995, “Fuzzy Sets and Fuzzy Logic: Theory and Applications”, Pearson Education.

Meggiolaro, M.A., Jaffe, P.C.L., Dubowsky, S., 1999, “Achieving Fine Absolute Positioning Accuracy in Large Powerful Manipulators”, Proc. of the International Conference on Robotics and Automation (ICRA '99), IEEE, Detroit, USA, pp.2819-2824.

Morel, G., Iagnemma, K., Dubowsky, S., 2000, “The Precise Control of Manipulators with High Joint Friction Using Base Force/Torque Sensing”, Automatica, pp. 931-941.

Ogata, K., 2002, “Modern Control Engineering”, Prentice Hall, 4th. edition.

Osborn, J.F., 1989, “Applications of Robotics in Hazardous Waste Management”, Proceedings of the SME 1989 World Conference on Robotics Research, Gaithersburg, MD, USA.

Shaffer, G. and Stentz, A., 1992, “A Robotic System for Underground Coal Mining”, Proceedings of the 1992 IEEE International Conference on Robotics and Automation, Vol.1, pp. 633-638.

Slotine, J.J., Li, W., 1991, “Applied Nonlinear Control”, Prentice-Hall.

Sujan, V.A., 2002a, “Optimum Camera Placement by Robot Teams in Unstructured Field Environments”, Proceedings of the IEEE International Conference on Image Processing (ICIP), Rochester, NY, USA.

Sujan, V.A., 2002b, “Task Directed Imaging in Unstructured Environments by Cooperating Robots”, submitted to the 2002 Third Indian Conference on Computer Vision, Graphics and Image Processing, Ahmedabad, India.

Sujan, V.A. and Dubowsky, S., 2002, “Visually Built Task Models for Robot Teams in Unstructured Environments”, Proceedings of the 2002 IEEE International Conference on Robotics and Automation, Washington, D.C., USA.

Takanishi, A., Tochizawa, M., Karaki, H. and Kato, I., 1989, “Dynamic Biped Walking Stabilized With Optimal Trunk And Waist Motion”, Proceedings of the 1989 IEEE/RSJ International Workshop on Intelligent Robots and Systems (IROS’89) - The Autonomous Mobile Robots and Its Applications, pp.187-192.